Journal of Alloys and Compounds 664 (2016) 580–589

Contents lists available at ScienceDirect

Journal of Alloys and Compounds

journal homepage: http://www.elsevier.com/locate/jalcom

Structural properties and the pressure-induced C → A phase transition of lanthanide sesquioxides from DFT and DFT + *U* calculations

D. Richard [a, *], L.A. Errico [a, b], M. Rentería [a]

[a] Departamento de Física and Instituto de Física La Plata (IFLP, CONICET), Facultad de Ciencias Exactas, Universidad Nacional de La Plata, CC 67, 1900 La Plata, Argentina
[b] Universidad Nacional del Noroeste de la Pcia. de Buenos Aires (UNNOBA), Monteagudo 2772, 2700 Pergamino, Argentina

ARTICLE INFO

Article history:
Received 31 July 2015
Received in revised form
20 December 2015
Accepted 28 December 2015
Available online 30 December 2015

Keywords:
Semiconductors
Phase transition
Ab initio
Structural properties
Lanthanide oxides
Bixbyite

ABSTRACT

Density functional theory (DFT) calculations were performed to analyze the structural properties of rare-earth lanthanide sesquioxides (Ln_2O_3) with the hexagonal A and the cubic C phases. The calculations were performed with the DFT-based Augmented Plane Wave plus local orbital (APW + lo) method, using both the local density approximation (LDA) and the Wu and Cohen parametrization of the generalized gradient approximation (WC-GGA) for the exchange and correlation energy. We also considered the addition of the Hubbard *U* term in the WC-GGA approximation (GGA + *U* approach), to take into account the strongly correlated Ln-4*f* electrons involved. The predicted equilibrium properties for both phases of each Ln_2O_3 system, i.e. crystal equilibrium volume, bulk modulus and its first pressure derivative are in good agreement with the corresponding experimental results. The obtained predictions with LDA and WC-GGA reveal that the A phase is stable for the lighter systems of the Ln_2O_3 sesquioxide series, and the C phase is favored for the heavier Ln_2O_3, in a qualitatively good agreement with the experimental data. However, the predicted C to A phase transition pressure $P_{C\rightarrow A}$, as well as the sesquioxide equilibrium volumes corresponding to the lanthanides of the middle of the series, underestimates the experimental values. The implementation of the *U* term gives a correct description of the insulating ground state of these systems, and also improves the predictions for the studied structural properties with respect to those predicted by LDA and WC-GGA. However, $P_{C\rightarrow A}$ is extremely sensitive to the *U* parameter, giving the GGA + *U* approach method very poor predictions for this quantity. The reasons of these effects are analyzed in detail.

1. Introduction

Lanthanide sesquioxides (Ln_2O_3, where Ln ranges from La to Lu) are currently extensively studied due to their potential application in a wide range of technological devices [1,2]. In this sense, they have recently gained attention for their potential application in luminescent materials [3], metal-oxide-semiconductor structures [4], radiation tolerant devices [5,6], and catalysts [7,8], among other uses.

Five different crystalline types for sesquioxides were identified. At temperatures lower than 2000 °C, depending on the radius of the cation, three polymorphs for Ln_2O_3 are commonly found: the hexagonal phase (*A*-type, space group P-3m1), the monoclinic phase (*B*-type, C/2m), and the cubic phase (*C*-type, Ia-3, also called bixbyite structure). On the other hand, above 2000 °C the phases designated as H or X are formed [9].

The study of the thermodynamic properties of lanthanide sesquioxides is of great significance [10]. Since practical applications of Ln_2O_3 could involve extreme pressure and temperature conditions, many recent investigations have been oriented to these subjects. So, among the wide range of studies of lanthanide oxides, those corresponding to the analysis of the structural properties under extreme pressure conditions become very relevant. Nowadays, X-ray diffraction (XRD) experiments allow a simultaneous precise determination of the lattice parameters and mechanical properties such as the bulk modulus (B) and its pressure derivative (B'). However, the results for these quantities in a certain compound

* Corresponding author.
E-mail address: richard@fisica.unlp.edu.ar (D. Richard).

http://dx.doi.org/10.1016/j.jallcom.2015.12.236
0925-8388/

depend on the experimental conditions. In this respect, the temperature and porosity dependence of the elastic properties of bulk rare earth sesquioxides has been matter of study over many years [11,12]. As a matter of example, different measurements for B over the Ln_2O_3 series gave values that ranges from 113 GPa (for A-La_2O_3 [13]) to 231 GPa (for A-Dy_2O_3 [14]). Recently, this kind of studies has also included nanosized sesquioxides [15–17].

The crystal structure of Ln_2O_3 can be altered under pressure. Because the C→B and the B→A phase transitions are accompanied by volume contraction, pressure tends to stabilize the A or B phases with respect to the C phase. In some cases, evidence of a direct C→A transition was recently observed for the first time [13,18,19]. In this respect, XRD and also Raman scattering experiments allowed the study of the C to A transition induced by high pressure under static load [15–24] or shock compression [25].

On the other hand, different DFT-based methods of calculation have been applied to the study of structural and mechanical properties of lanthanide oxides [26–28]. In these studies, the exchange and correlation potential was usually treated by using the local density approximation (LDA) or the generalized gradient approximation (GGA). The stability of the C and A Ln_2O_3 phases were theoretically studied using the projector-augmented wave (PAW) method [26]. Recently, first-principles systematic investigations of the structural properties of lanthanide dioxides (LnO_2 [27]) and monoxides (LnO [28]) have also been presented. This kind of studies usually also attends to the electronic properties of the selected systems by analyzing the density of electronic states (DOS). In the last few years, many researchers have intended to improve the *ab initio* methods in order to account for the lanthanide strongly correlated 4*f* electrons involved in such systems [29–31]. In this respect, the inclusion of a Hubbard U term in the common DFT approaches such as the LDA is frequently done (LDA + U method).

In a recent paper, we presented an Augmented Plane Wave plus local orbital (APW + lo) study of the electronic, structural, and hyperfine properties in pure and Cd doped C-Ln_2O_3 [31]. In particular, we analyzed the electric-field-gradient (EFG) at the cationic sites of the studied systems. We showed that the capability of the LDA + U method to correctly predict the insulating ground state for the entire C-Ln_2O_3 series does not always guarantee a good reproduction of the experimental EFG. In that work the study of structural properties in the pure systems were restricted to the prediction of the equilibrium atomic internal positions, with the lattice parameters fixed at the experimental values. In the doped systems, we analyzed the structural and electronic modifications induced by the Cd impurity to the C-Ln_2O_3 semiconducting host. So, we did not delve into the study of other Ln_2O_3 structures than the cubic phase, and we neither investigated other structural properties beyond the atomic internal positions, such as the equilibrium lattice parameters or the bulk modulus.

In this paper we present a detailed study from first principles of the structural properties for both the C phase and the A phase of the Ln_2O_3 series. Using the APW + lo method, we systematically calculate the equilibrium volume and the bulk modulus for both phases, and the predicted C→A transition pressure in each Ln_2O_3 system over the sesquioxide series. We also analyze how these properties are affected by introducing the Hubbard U parameter. As mentioned before, recent experimental measurements show a direct C→A transition in some Ln_2O_3 compounds. Hence, a predictive model that could describe the structural properties mentioned above could help to better understand the role played by the 4*f* electrons in the lanthanide sesquioxides.

The organization of this paper is as follows: in Section 2 we introduce the structure of Ln_2O_3 A and C phases. In Section 3 we describe the method of calculation, and in Section 4 we present our results. Finally, in Section 5 we discuss the results and the conclusions are drawn.

2. Lanthanide sesquioxide structures

The Ln_2O_3 hexagonal A-type structure has a lattice parameter ratio $c/a \approx 1.55$. Its unit cell contains one Ln_2O_3 formula unit (see Fig. 1a). In this structure, there are one inequivalent Ln atom and two types of oxygen atoms (O1 and O2 in what follows). Each unit cell contains a O1 atom located at the origin of the cell (equivalent to 1*a* in Wyckoff notation), and two equivalent O2 atoms at the internal coordinates ±(1/3, 2/3, v) (2*d* in Wyckoff notation). The O1 and O2 atoms have different Ln coordination: the O1 atom is surrounded by six Ln atoms (Fig. 1b), while the O2 atoms are found in the center of a tetrahedron of four Ln atoms (Fig. 1c). On the other hand, the Ln atoms are located at positions 2*d*, with internal coordinates ±(1/3, 2/3, u), and are coordinated with seven nearest oxygen neighbors (ONNs, see Fig. 1d). So, the internal parameters v and u determine the positions of all the atoms in each A-Ln_2O_3 system [32].

The unit cell of the cubic C-type structure contains 16 Ln_2O_3 formula units (Fig. 2a). It presents an inequivalent crystallographic site for the oxygen atoms, and two inequivalent sites for cations, called LnD and LnC. All oxygen sites are coordinated by four Ln atoms (see Fig. 2b), while the LnD and LnC sites are both coordinated with six ONNs (see Fig. 2c and d, respectively). For the LnD site, each of the six ONNs that surrounds the Ln atom lies at the corners of a distorted cube, with two opposite corners on a cube diagonal unoccupied, and are equidistant to it. In the LnC site, each of the six ONNs around the cation occupies the corner of a more distorted cube, with the corners of a face diagonal of such cube unoccupied. In this case there are three different pairs of LnC-ONN distances. The internal positions of the atoms in the unit cell are determined by the parameters u, x, y, and z, where u determines the positions of LnC cations, and x, y, and z determine those of the oxygen atoms [32].

The structural properties of the Ln_2O_3 oxides are affected by the presence of their inner Ln-4*f* electron-shell. In this sense, the Ln_2O_3 oxide series evolves with the gradually filling of the Ln-4*f* electron shell, starting with La_2O_3, where the La atom has the electronic configuration [Xe] $4f^0\ 5d^1\ 6s^2$. As the electrons are added to the 4*f* orbitals, the initial shielding provided by this shell over the nuclear charge is lessened, and the outer $5d^1$ and $6s^2$ valence electrons experience an increasing coulombic attraction towards the nucleus. This effect is the so-called *lanthanide contraction*: the larger is the number of 4*f* electrons, the smaller the Ln radius. In addition, the trivalent valence state is preferred for the Ln atom [9]. Thus, the ionic size of the Ln atom in combination with oxygen is such for the formed Ln_2O_3 oxides that the unit cell volume decreases with increasing Ln atomic number (Z_{Ln}).

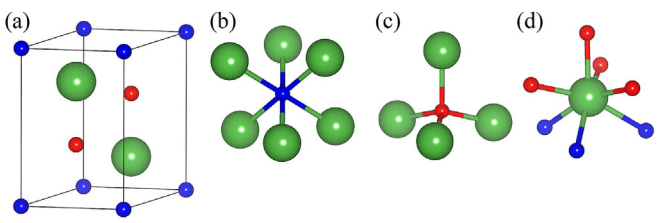

Fig. 1. (a) A-Ln_2O_3 unit cell and (b–d) the nearest-neighbors coordination of their crystallographic sites. The big green spheres stand for the Ln atoms, while the small spheres represent the O1 and O2 atoms (blue and red spheres, respectively). (For interpretation of the references to color in this figure legend, the reader is referred to the web version of this article.)

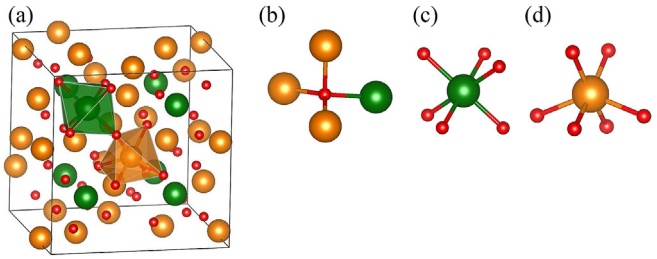

Fig. 2. (a) *C*-Ln_2O_3 unit cell and (b–d) the nearest-neighbors coordination of their crystallographic sites. The small red spheres represent the O atoms, while the big spheres stand for the LnD and LnC atoms (green and orange, respectively). In Fig. 1a the polyhedra help to visualize the coordination of the two non equivalent cationic sites. (For interpretation of the references to color in this figure legend, the reader is referred to the web version of this article.)

Under compression, a direct C → A transformation for some Ln_2O_3 sesquioxides has been recently observed, which is accompanied by a volume contraction of about 10% [13,18,19]. In these cases, the phase transition pressure $P_{C\rightarrow A}$ at room temperature tends to increase with increasing Z_{Ln}, i.e. $P_{C\rightarrow A}$ increases with decreasing the Ln_2O_3 cation radius [13,23]. This transformation is accompanied by a change in the number of Ln's ONNs from six to seven (as shown in Figs. 1 and 2).

3. Method of calculation

The present calculations were performed with the WIEN2k implementation of the APW + lo method [33]. The exchange and correlation potential was treated using both the LDA approximation [34] and the Wu and Cohen parametrization of the generalized gradient approximation (WC-GGA) [35].

The muffin-tin radii (R_{MT}) used for the cations and the O atoms were 1.03 and 0.90 Å, respectively. The wavefunctions in the interstitial region were expanded in planewaves using a cutoff parameter $R_{MT}K_{max} = 9$, where K_{max} is the maximum modulus for the reciprocal lattice vector, and R_{MT} in this expression stands for the smallest atomic muffin-tin sphere radius. Integration in the reciprocal space was performed using the tetrahedron method, taking up to 100 *k*-points in the first Brillouin zone. We checked that these parameters gave well converged predictions. In each case, the self-consistent calculation was achieved by considering a total energy tolerance of 0.1 mRy.

For all the *A*-Ln_2O_3 and *C*-Ln_2O_3 structures the total energies were calculated self-consistently considering different values for the unit cell volume *V* around the experimental value. In this respect, the chosen R_{MT} radii allow a volume reduction of about 20% with respect to its experimental value. The Birch–Murnaghan equation of state (EOS) was fitted to the obtained energy vs. volume data ($E(V)$) to determine the equilibrium structural properties of each compound, i.e., the equilibrium volume V_0, the bulk modulus *B*, and its derivative with respect to pressure, *B'* [36]. In the case of the Ln_2O_3 systems with A-type structure, we fixed the lattice parameter ratio *c/a* at its experimental value to perform this $E(V)$ data analysis. Even so, we previously performed additional calculations in several *A*-Ln_2O_3 systems to confirm that the predicted *c/a* value only differs from the experimental one in less than 1%. For example, in the case of *A*-La_2O_3, such difference is lower than 0.2% [37]. For the present calculations, in the cases where no experimental lattice parameters have been reported, we used those corresponding to the sesquioxide with the nearest Z_{Ln} value.

In order to study the structural phase stability, we need to calculate Gibb's free energy *G* for the two phases, given by $G = E + PV\text{-}TS$. But since the calculations are performed at 0 K, Gibb's free energy is equal to the enthalpy $H = E + PV$. Then, for a given sesquioxide and a given pressure, the most stable structure is that with the lowest value of *H*. So, we compare A-phase and C-phase enthalpies in order to determine the $P_{C\rightarrow A}$ phase transition pressure for each Ln_2O_3 system.

Finally, to improve the description of the strongly correlated Ln-4*f* electrons, we employed the spin-polarized WC-GGA approximation plus the Hubbard *U* term in the self-interaction-corrected scheme (GGA + *U* approach), which corresponds to the method described in Refs. [38,39] but using the WC-GGA approximation instead of LDA. We took $U = 0.8$ Ry (10.9 eV) for the Ln-4*f* orbitals. This choice was performed considering the good description of the electron density of states we already obtained in Ref. [31]. In this respect, we have to mention that the development of more sophisticated DFT + *U* methods is still a subject of study [40]. In this work we will analyze the predicted structural properties using the GGA + *U* approach, and how the *U* parameter affects these quantities for the A and C phases.

4. Results

4.1. LDA and WC-GGA approximations

For the A and C structures of each Ln_2O_3 system we determined the equilibrium volume V_0, the bulk modulus *B* and its derivative with respect to pressure *B'* by fitting the Birch–Murnaghan EOS to the $E(V)$ data predictions. As an example, in Fig. 3 we present the $E(V)$ curves corresponding to the LDA predictions in Lu_2O_3 for both phases. The obtained structural properties for each Ln_2O_3 system with the A and C structures are presented in Table 1. In this table we also have included previous experimental room temperature results obtained by other authors. Our results are also graphically presented in Fig. 4, using blue (in the web version) blank squares and red blank circles for the LDA and WC-GGA results, respectively. As can be seen for both structures, V_0 decreases with Z_{Ln}, showing that the APW + lo method correctly describes the *lanthanide contraction* effect on the unit cell volume of the Ln_2O_3 compounds. Each approximation predicts that, for a same Ln_2O_3 system, the A structure occupy about 10% less volume than the C structure. For both structures, the LDA and WC-GGA approximations predict a unit cell volume lower than the experimental one (which are represented in Fig. 4 by solid circles). The largest differences between our predictions and the experimental values are found near the

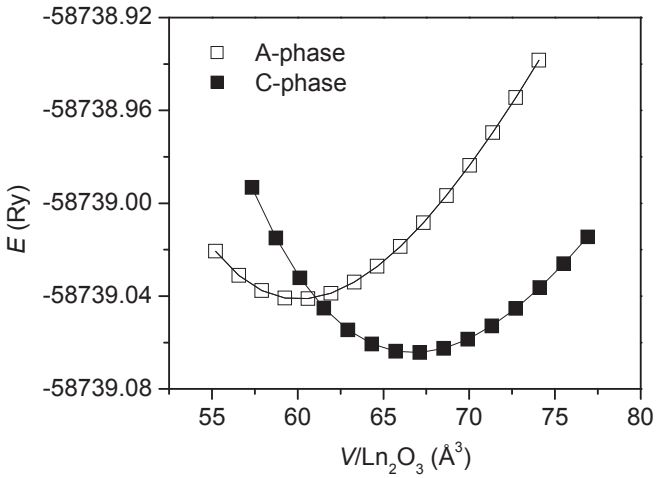

Fig. 3. $E(V)$ data for Lu_2O_3, calculated by LDA. The solid lines are the Birch–Murnaghan EOS fits. The obtained structural parameters are presented in Table 1.

Table 1
Predicted equilibrium volume V_0 per formula unit, bulk modulus B, and its pressure derivative B', for the A and C structures of each Ln_2O_3 system. The phase transition pressure $P_{C\to A}$ is also included for LDA and WC-GGA approximations. The listed experimental results have been taken from the indicated references. The experimental volumes indicated with an asterisk come from an extrapolation to zero pressure, while the values of indicated with a double asterisk corresponds to quantities that were kept fixed during the fitting procedure. The intervals in experimental $P_{C\to A}$ pressures indicate the region of certainty in which the phase transition is thought to be produced.

		A-phase			C-phase			$P_{C\to A}$ (GPa)
		V/Ln_2O_3 (Å^3)	B (GPa)	B'	V/Ln_2O_3 (Å^3)	B (GPa)	B'	
La_2O_3	LDA	76.58	155.2	4.34	87.77	133.9	4.15	0.0
	WC-GGA	78.60	144.6	4.36	89.98	125.6	4.15	−1.1
	GGA + U	79.91	142.8	4.39	91.39	124.4	4.18	
	Exp.	82.296 [32]	113(1) [13]	6.0(1) [13]	92.1 [32]			
		82.240 [13]						
Ce_2O_3	LDA	71.65	166.8	4.45	80.44	148.5	5.62	−2.6
	WC-GGA	73.60	155.0	4.48	82.83	135.8	4.46	−1.0
	GGA + U	79.51	142.0	4.29	88.19	135.5	4**	
	Exp.	79.45 [32]			86.9 [9]			
Pr_2O_3	LDA	69.00	170.6	4.38	77.87	148.2	4.46	−3.9
	WC-GGA	71.01	159.0	4.13	80.09	137.0	4.36	−2.2
	GGA + U	76.15	152.3	4**	86.08	157.9	4**	
	Exp.	77.01 [32]			86.6(2) [41]			
Nd_2O_3	LDA	67.18	173.5	4.43	75.77	150.5	4.38	−3.7
	WC-GGA	69.22	159.8	4.48	78.11	136.9	4.34	−1.9
	GGA + U	74.82	155.1	3.62	85.01	122.0	5.45	
	Exp.	76.15 [32]	135.6 [42]		84.9(3) [41]			
Pm_2O_3	LDA	65.76	176.2	4.50	73.95	153.8	4.50	−2.7
	WC-GGA	67.86	160.8	4.53	76.47	136.0	5.10	−0.9
	GGA + U	74.20	156.1	4.01	82.87	129.0	4**	
	Exp.				83.0(2) [41]			
Sm_2O_3	LDA	64.30	177.4	4.42	72.46	153.4	4.22	−1.0
	WC-GGA	66.50	159.0	4.59	75.01	136.5	4.38	1.2
	GGA + U	72.31	147.0	4.49	81.09	138.3	4.29	
	Exp.	72.1(3) [18]	224(23) [18]	1.5(7) [18]	81.129 [43]	142(3) [18]	4** [18]	7.5–12.5 [18]
		73* [13]	130(1) [13]	6.9(1) [13]	81.9** [18]	116(1) [13]	4** [13]	4.0(1.5) [13]
			155(5) [44]		81.684 [13]	149(2) [44]		
Eu_2O_3	LDA	63.41	177.7	4.39	71.28	156.1	4.33	0.5
	WC-GGA	65.59	158.3	4.95	73.84	137.0	4.59	2.6
	GGA + U	72.81	134.3	4**	79.61	143.1	4.17	
	Exp.	72* [13]	134(1) [13]	4.1(1) [13]	79.269 [43]	115(1) [13]	5.9(4) [13]	6.0(1.5) [13]
					80.030 [13]			
Gd_2O_3	LDA	62.92	178.1	4.32	70.30	158.3	4.42	−0.7
	WC-GGA	65.17	160.7	4.42	72.81	139.7	4.77	1.3
	GGA + U	70.18	160.7	4.39	78.48	144.7	4.24	
	Exp.	71* [13]	142(14) [19]	6(4) [19]	78.666 [43]	118(21) [19]	14(8) [19]	4.6–5.2 [25]
			160(21) [20]	4** [20]	79.0(2) [15]	188(25) [20]	4** [20]	6.78–10.97 [15]
			174(11) [21]	4** [21]	79.155(4) [20]	134(6) [21]	4** [21]	12.4 [19]
			145(1) [13]	4.2(1) [13]	79.015 [13]	125(1) [13]	4.7(1) [13]	7–14.7 [20]
								8.9–14.8 [21]
								7.0(1.5) [13]
								12.62–16.51 [16]
Tb_2O_3	LDA	62.27	179.5	4.22	69.48	158.6	4.31	−0.3
	WC-GGA	64.54	160.3	4.47	71.97	143.7	4.28	2.3
	GGA + U	69.08	159.9	4.53	77.13	139.0	4.67	
	Exp.				77.21(2) [9]			
Dy_2O_3	LDA	61.70	180.9	4.24	68.72	159.9	4.37	1.5
	WC-GGA	63.96	165.5	4.09	71.16	145.3	4.35	3.8
	GGA + U	67.33	160.4	4.64	75.26	148.9	5.14	
	Exp.		231(22) [14]	3.5(6) [14]	75.94(1) [45]	150 [46]	2.8(7) [14]	14.6–17.8 [17]
						191(4) [14]		
Ho_2O_3	LDA	61.31	180.9	4.63	68.13	161.6	4.50	3.4
	WC-GGA	63.57	163.6	4.49	70.57	145.7	4.42	5.3
	GGA + U	66.48	179.1	3.71	73.90	152.0	4.48	
	Exp.		204(19) [47]	3.8(5) [47]	74.57(4) [45]	127 [11]	4 [22]	9.5–16 [22]
						134 [46]	4.8(4) [47]	
						178 [22]	4 [48]	
						206(3) [47]		
						178(7) [48]		
Er_2O_3	LDA	61.12	180.4	4.64	67.73	161.2	4.46	5.7
	WC-GGA	63.38	162.2	4.66	70.16	146.1	4.46	7.0
	GGA + U	65.35	173.6	4.51	72.44	157.2	3.98	
	Exp.				73.39 [49]	155 [11]	8.4 [50]	14.0(1.5) [13]
					73.265 [13]	140 [46]	5.9(1) [13]	
						200(6) [50]		
						136(1) [13]		
Tm_2O_3	LDA	60.98	178.5	4.56	67.52	161.6	4.40	7.0
	WC-GGA	63.24	160.7	4.62	69.95	146.6	4.38	8.5
	GGA + U	64.04	168.4	4.65	71.35	157.7	4.36	
	Exp.				72.0(2) [41]	143 [51]	4 [48]	
						130 [46]		
						154.5(7.5) [48]		

(*continued on next page*)

Table 1 (*continued*)

		A-phase			C-phase			$P_{C\to A}$ (GPa)
		V/Ln_2O_3 (Å^3)	B (GPa)	B'	V/Ln_2O_3 (Å^3)	B (GPa)	B'	
Yb_2O_3	LDA	60.93	177.8	4.61	67.48	161.6	4.52	7.5
	WC-GGA	63.21	160.1	4.61	69.93	144.5	4.62	9.1
	GGA + U	63.15	178.7	4.33	70.22	160.9	4.27	
	Exp.				70.969 [49]	181(1) [52]	7.3(2) [52]	17.0(1.5) [13]
								11.3–20.6 [24]
Lu_2O_3	LDA	60.05	198.8	4.33	66.73	179.4	4.30	7.7
	WC-GGA	62.12	182.2	4.39	68.93	164.8	4.31	9.4
	GGA + U	62.40	179.9	4.29	69.30	163.0	4.29	
	Exp.				69.994 [43]	144(1) [13]	6.7(1) [13]	14.0(1.5) [13]
					70.128 [13]	214(6) [53]	9(1) [53]	
						113.5(7) [54]	1.7(3) [54]	

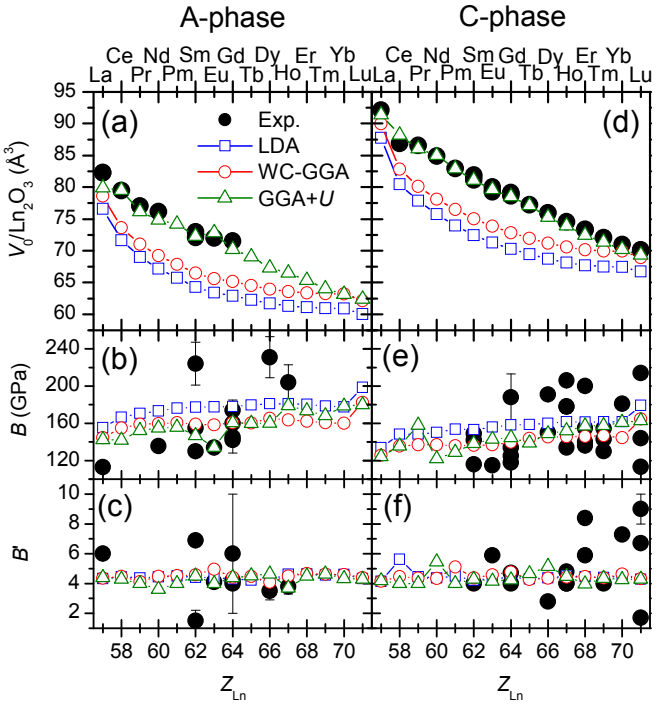

Fig. 4. Predicted equilibrium volume V_0 per formula unit, bulk modulus B, and its pressure derivative B' as a function of the atomic number Z_{Ln} of Ln_2O_3 cation for (a–c) the A structure and (d–f) the C structure. The corresponding Ln atom label is indicated on the top. The solid circles are experimental results (see Table 1). The GGA + U calculations used $U = 0.8$ Ry.

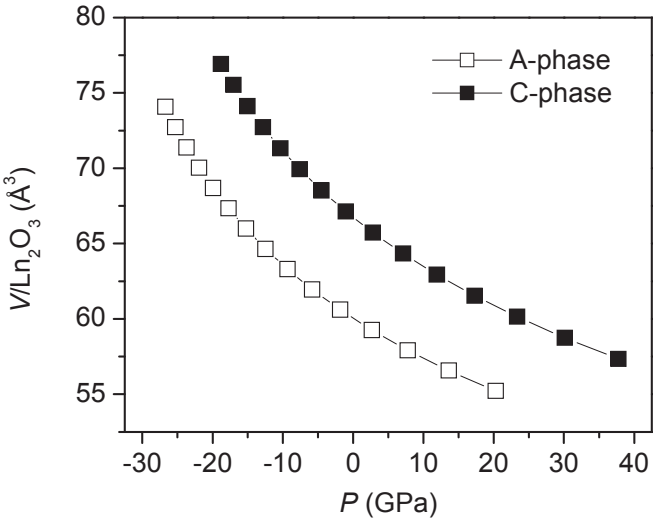

Fig. 5. $V(P)$ data for the A and C phases of Lu_2O_3, calculated by LDA.

middle of the series (cations Pm to Gd), where they can reach up to 14% of the experimental volume (this corresponds to a 2% difference in the lattice parameters). We also found that WC-GGA predicts V_0 values systematically larger than LDA (about 3% larger), in a better agreement with the experimental results. These differences between the two approximations and between calculations and experiments are within the precision range of the different approaches [55].

Under pressure, both approximations predict that each structure undergoes a volume decrease, maintaining a nearly constant volume difference between phases over all the studied pressure range. In this respect, in Fig. 5 we present as an example the $V(P)$ data corresponding to the LDA predictions in both the A and the C phase of Lu_2O_3.

Regarding the bulk modulus, we found an increase of B with Z_{Ln} for both structures, in such a way that B increases in about 30% from La_2O_3 to Lu_2O_3 (see Fig. 4b and e). The WC-GGA approximation gives values systematically lower that those predicted by LDA, being their difference of about 10% with respect to the LDA approximation. On the other hand, for each Ln_2O_3 system we obtained a B value for the A structure 10–15% higher than that of the C structure (see Table 1). These increasings of B are consequence of the more compact structure that the sesquioxide has in the A phase, or, for a same phase, as Z_{Ln} increases. When we compare our predictions with the different experimental room temperature measurements (which, as we mentioned above, are rather disperse, see the solid circles in Fig. 4b and 4e), both approximations seem to be in quite good agreement with the experimental determinations. Additionally, the predicted pressure derivatives B' practically do not depend on Z_{Ln}, being its value near 4.5 for both structures. This result is also in a general good agreement with the experimental data (see Table 1).

Finally, in addition to the calculation of V_0, B, and B', we determine the $P_{C\to A}$ phase transition pressure from the $H(P)$ curves for each sesquioxide. In Fig. 6 we present as an example the $H(P)$ data for Lu_2O_3. At the transition pressure the enthalpies for the two phases must be equal. In Table 1 we included the predicted $P_{C\to A}$ phase transition pressures by using the LDA and WC-GGA approximations. These results are also graphically presented as a function of Z_{Ln} in Fig. 7. As can be seen, the two approximations

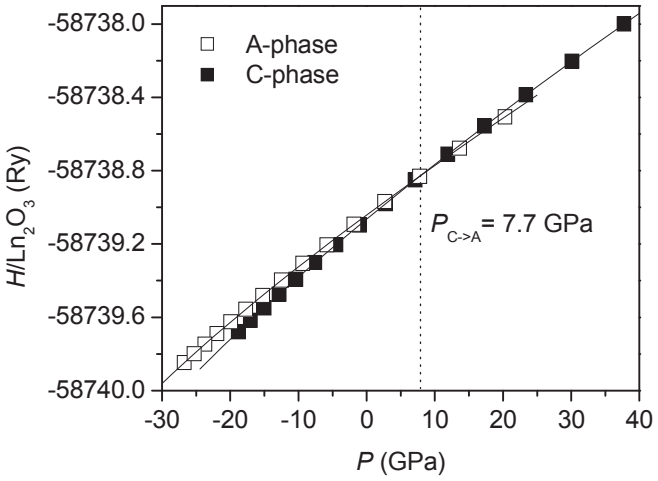

Fig. 6. $H(P)$ data for Lu_2O_3, calculated by LDA. The solid lines are polinomial fits used to interpolate the data and determine the $P_{C\rightarrow A}$ phase transition pressure (at the vertical dotted line).

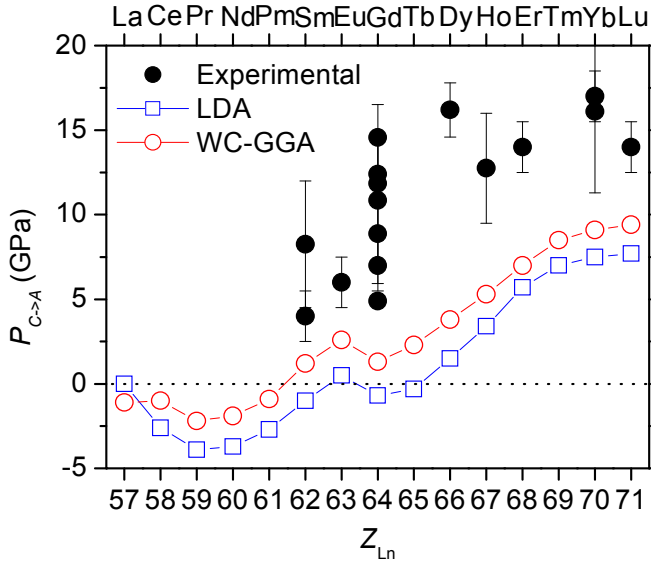

Fig. 7. Predicted $P_{C\rightarrow A}$ phase transition pressure as a function of Ln_2O_3 cation's atomic number Z_{Ln}. The solid circles correspond to experimental results.

show the same trend for $P_{C\rightarrow A}$ with increasing Z_{Ln}. Our calculations give a negative $P_{C\rightarrow A}$ pressure up to Sm_2O_3 or Eu_2O_3 (depending on the approximation). Also, the WC-GGA approximation gives $P_{C\rightarrow A}$ pressures about 2 GPa higher than LDA (with the only exception of La_2O_3, where the LDA $P_{C\rightarrow A}$ pressure is larger than that of WC-GGA). These results show that not all the studied sesquioxides are stable in the C structure: only for those cases where $P_{C\rightarrow A}$ is positive we theoretically predict the Ln_2O_3 system in the C structure. Our predicted $P_{C\rightarrow A}$ values underestimate the available experimental determinations (see the solid circles in Fig. 7), but indicate that the C-type structure is stable for the sesquioxides with larger Z_{Ln} (from Sm_2O_3–Eu_2O_3 to Lu_2O_3), and the A-type structure is preferred for the lower Z_{Ln} ones. This result is in good agreement with the experimental relative stability of these polymorphic forms [9].

The dependence of the calculated $P_{C\rightarrow A}$ with Z_{Ln} is consistent with the predictions obtained for V_0 and B mentioned above: as the sesquioxide becomes denser, the larger is the value of B, and the larger is the pressure required to transform the structure from the C to the A phase.

Additionally, in the A phase the Ln cations have larger oxygen coordination in comparison to the C phase, which means that the 4*f* electrons would be more delocalized in the hexagonal phase. In consequence, for the heavier Ln_2O_3, where the 4*f* electrons are more localized, we will need higher pressures to reach the delocalization condition and, therefore, the A structure. Hence, we can understand why higher pressures are needed to transition from the C to the A structure as Z_{Ln} increases.

The underestimation of the $P_{C\rightarrow A}$ values is a consequence of the failure of the LDA and WC-GGA approximations to correctly describe the strongly correlated Ln-4*f* electrons. In this regard, in the next section we will see how the inclusion of the U parameter promotes the 4*f* electron localization, and the effects that it has on the structural parameters and the transition pressure.

4.2. GGA + U approach

For all the Ln_2O_3 systems in which the Ln-4*f* orbital is partially filled, LDA and WC-GGA predict a metallic ground state, as shown in Ref. [31]. In these cases, a partially filled band with Ln-4*f* character is found in the density of states (DOS). Otherwise, for La_2O_3 and Lu_2O_3, where the cation 4*f* band is completely unfilled and filled, respectively, the predicted system is an insulator, in agreement with the experimental conductivity behavior. The application of the Hubbard U term modifies the DOS. For the sesquioxides with the Ln-4*f* band partially filled, the application of the Hubbard U parameter splits this band into two energy regions: the occupied 4*f* states are pushed to lower energies, and the unoccupied 4*f* states are shifted to higher energies. To show this effect, in Fig. 8 we present as an example the DOS for *A*-Nd_2O_3 for different values of U. For $U = 0$ Ry, we found a partially filled Nd-4*f* band, between a filled band with O-2*p* character and the empty bands with Nd-4*f* and Nd-5*d* character (Fig. 8a). For nonzero U, the occupied Nd-4*f* states are separated from the unoccupied Nd-4*f* states by an energy difference equal to U, and the resulting system becomes an insulator.

By using a Hubbard parameter of 0.4 Ry or higher it is possible to distinguish a valence band with a predominantly O-2*p* character and a conduction band with its lower energy region mainly due to Ln-5*d* states. Both bands are separated by about 4 eV (as shown in Fig. 8c–e for *A*-Nd_2O_3). So, the GGA + U approach with a nonzero U value correctly describes the insulating character of this kind of systems.

The improvement on the description of the DOS obtained with the GGA + U approach is also accompanied by better predictions of the structural properties with respect to those predicted by LDA and WC-GGA. In this sense, the inclusion of U = 0.8 Ry in Ln-4*f* orbitals drastically improves the prediction for the unit cell volumes. In Table 1 we have included the predictions for V_0, B and B' obtained with the GGA + U approach. As can be seen, the differences between the predicted and the experimental volumes are reduced to below 2% of the experimental value (see Fig. 4, green blank triangles).

On the other hand, the GGA + U approach predicts B and B' values that maintain nearly the same dependences on Z_{Ln} than those obtained with the LDA and WC-GGA approximations (see Fig. 4b and e).

According to our results, the improvements in the V_0 prediction obtained with the GGA + U approach are especially important in those sesquioxides where the cation has the 4*f* band partially filled. In this respect, we also studied the dependence on U for V_0 by performing additional calculations. The pass from WC-GGA to the bare spin-polarized calculation (*i. e.*, GGA + U using $U = 0$) slightly increases the prediction for V_0. Next, we found that when we apply

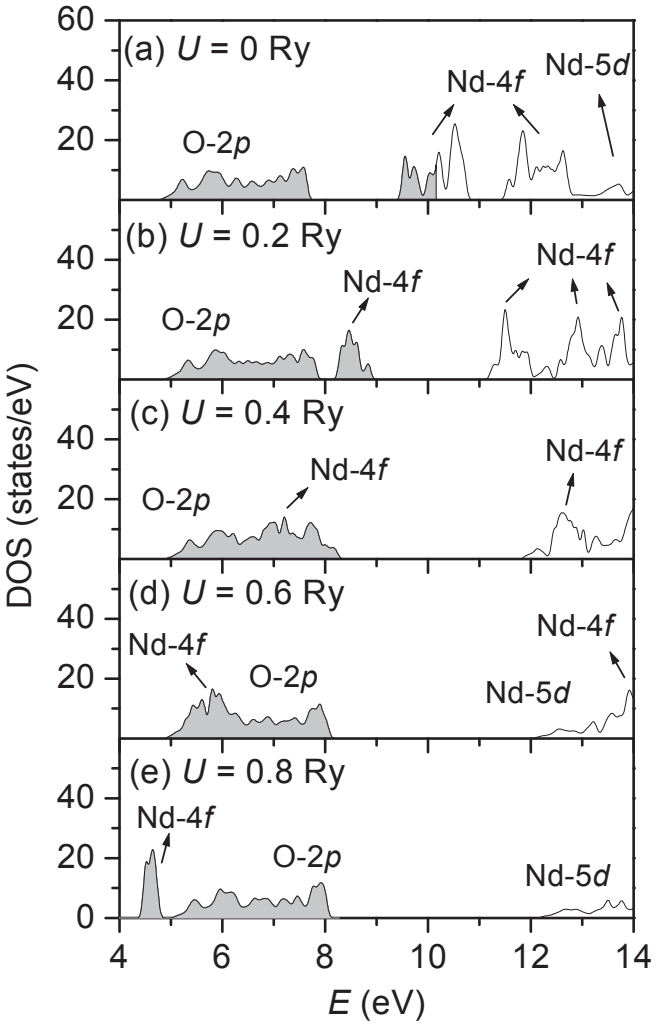

Fig. 8. DOS of A-Nd_2O_3 as a function of U in the GGA + U approach. Shaded areas indicate occupied energy states.

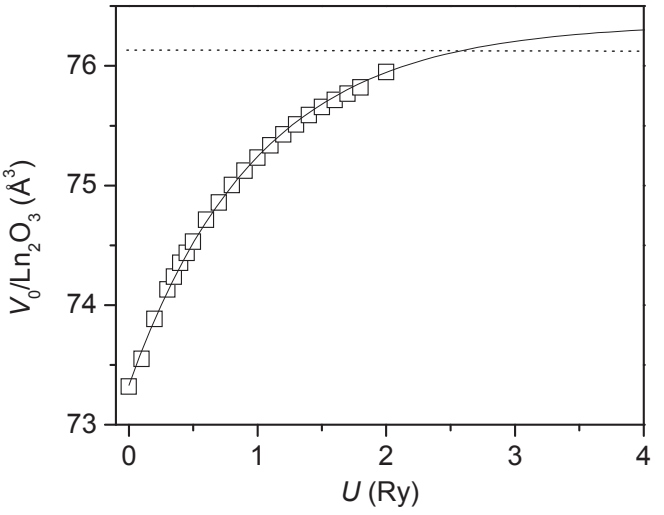

Fig. 9. $V_0(U)$ data for A-Nd_2O_3, calculated by GGA + U. The solid line is the fit of the exponential form $V_0(U) = a\text{-}be^{-U}$. The horizontal dotted line stands for the corresponding experimental volume.

U values ranging from 0 to 0.8 Ry the predicted V_0 increases almost linearly for the both considered structures, reaching the values already presented in Table 1 for $U = 0.8$ Ry. This behavior is due to a gradual change in the hybridization between the Ln-4f and the O-2p states that it is produced when we vary the U term. For higher values of U, the predicted V_0 asymptotically reaches a maximum value. As an example, in Fig. 9 we present the $V_0(U)$ data for A-Nd_2O_3. It can be seen that V_0 tends asymptotically to a value about 1% greater than the experimental one (as the fitted curve predicts). This is in agreement with the abrupt loss of the mentioned hybridization once the Ln-4f filled band is completely displaced below the valence band (see Fig. 8). For higher values of U, the mentioned hybridization becomes negligible, the occupied Ln-4f band moves even more to deeper energies and becomes narrower, and the Ln-4f orbitals adopt a more pronounced atomic-like character. We additionally studied the $V_0(U)$ curve in other systems, and we found the same behavior: V_0 tends to a value up to 3% greater than the experimental value.

In Fig. 10 we plot different projections of the electron density $\rho(\mathbf{r})$ at the (110) plane in A-Nd_2O_3, which contains the Ln, O1, and O2 atoms on the same plane. These plots show the projections for the total $\rho(\mathbf{r})$, the electron density for the states corresponding to the valence states $\rho^{val}(\mathbf{r})$, and the density for the occupied Nd-4f band states $\rho^{f}(\mathbf{r})$, when $U = 0$ Ry (Fig. 10a–c) and $U = 0.8$ Ry (Fig. 10d–f). In the case of Fig. 10b, the $\rho^{val}(\mathbf{r})$ density corresponds to the occupied O-2p states (those in the 5–8 eV energy range, as showed in Fig. 8a). According to the total $\rho(\mathbf{r})$ plots, an extremely small degree of covalence between Nd and O atoms exist for both values of U. The $\rho^{val}(\mathbf{r})$ projections show the strong O-2p character of the valence band (Fig. 10b and e). The scale in these graphs allows the visualization of the slight change on the distribution of the Nd-4f states that contribute to this band when the U parameter is applied. Also, the $\rho^{f}(\mathbf{r})$ projections reveal the effect of the U parameter on the spatial distribution of the Nd-4f electrons. As we mentioned before, when $U = 0.8$ Ry the 4f states adopt a more pronounced atomic-like character.

Finally, we found that for those sesquioxides where the cation has the 4f band partially filled, the GGA + U prediction for $P_{C\to A}$ is extremely sensitive to the U parameter. This is due to the fact that in each structure the $E(V)$ data have a different behavior when we include the U correction. Although these data can be described by using B and B' values similar to those obtained with LDA and WC-GGA (see Table 1), the application of U produces a displacement of the (V_0, E_0) coordinates of the $E(V)$ minimum, which is different depending on the structure (A or C) considered. These displacements are particularly important in those systems with the Ln-4f shell partially filled. In consequence, for each Ln_2O_3 system we found a relative movement of the H(P) curves for the C-phase and the A-phase that strongly modifies the predicted value for $P_{C\to A}$. For example, for Ho_2O_3 we observe that E_0 tends to increase faster for the C-phase than for the A-phase as U increases from 0 to 0.8 Ry. At the same time, the V_0 values for both phases have similar increasing rates with U. Therefore, the H(P) curve of the C-phase moves up with increasing U faster than that of the A-phase, and $P_{C\to A}$ drastically decreases with U, in a way that it covers an order of magnitude when U ranges from 0 to 0.8 Ry. As an example of this effect, in Fig. 11 we present the $H(P)$ curves for Ho_2O_3 for $U = 0.2$ and 0.8 Ry, where we found $P_{C\to A} = -1.2$ and -18 GPa, respectively. If we compare with the $P_{C\to A}$ predicted value of 6.3 GPa obtained using WC-GGA, or with the experimental range 9.5–16 GPa (see Table 1), we confirm that the methodology employed here for selecting the U parameter in the GGA + U approach gives poor accuracy in the prediction of $P_{C\to A}$. For this reason, we have omitted in Table 1 the $P_{C\to A}$ values corresponding to this approximation.

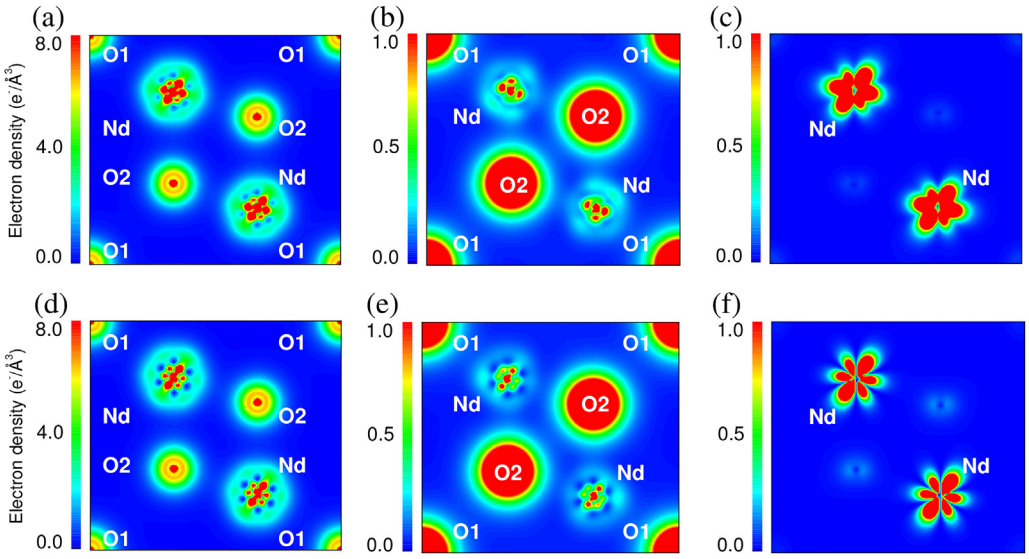

Fig. 10. Total electron density $\rho(\mathbf{r})$ (on the left) and its projections $\rho^{val}(\mathbf{r})$ (middle) and $\rho^{f}(\mathbf{r})$ (on the right) for *A*-Nd_2O_3 in the (110) plane, using (a–c) $U = 0$ Ry, and (d–f) $U = 0.8$ Ry. Different scales were used to optimize visibility in each graph.

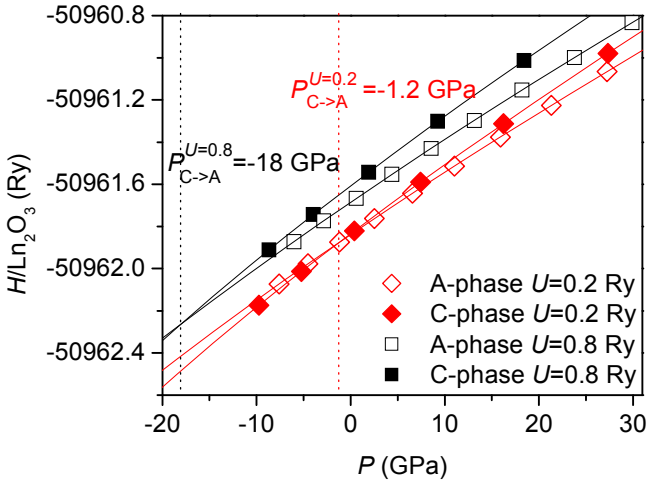

Fig. 11. H(P) data for Ho_2O_3, calculated by GGA + U, for $U = 0.2$ Ry (in rhombuses) and $U = 0.8$ Ry (in squares). The solid lines are polinomial fits used to determine the $P_{C\to A}$ phase transition pressure.

5. Discussion and conclusions

Using the APW + lo method we have systematically studied the electronic structure and the structural properties of the complete series of Ln_2O_3 sesquioxides in the A and C crystal structures. We obtained that each Ln_2O_3 in the A structure occupy about 10% less volume (per formula unit) than the volume it has in the C structure. This result is in good agreement with the experimental measurements. Also, we have theoretically predicted the decrease of the equilibrium volume V_0 with increasing the lanthanide atomic number Z_{Ln}, which is an effect of the *lanthanide contraction*. Previous theoretical studies have also predicted this behavior of V_0 with Z_{Ln} using other methods of calculation [29,56]. In our case, the LDA and the WC-GGA approximations underestimate the experimental volumes in about 10%, a difference that is expected considering the error of the approximations to the exchange and correlation energy [55]. Also, both approximations give a bulk modulus B that increases with Z_{Ln} for both the A and C structures. This predicted dependence of B with Z_{Ln} is also a reflection of the *lanthanide contraction*, because the shielding of the [Xe] electronic core of the lanthanides varies in a gradual manner as electrons are added to the 4*f* shell. Therefore, the bulk properties of the Ln_2O_3 oxides also vary gradually through the sesquioxide series. So, as we mentioned above, the contraction of the cationic radii with Z_{Ln} causes the increase on the sesquioxide bulk density (i.e., the decrease in V_0), and the increase in B.

Regarding the $P_{C\to A}$ phase transition pressures for the Ln_2O_3 systems, up to our knowledge the work of Rahm et al. is the only previous theoretical study that investigated on this subject [26]. In that work, the authors used the PAW method and treated the Ln-4*f* orbitals as core states, in the core state model (CSM) approach. In that case, there were obtained similar $P_{C\to A}$ results to those presented here, predicted by the APW + lo method. The $P_{C\to A}$ values increases with Z_{Ln}, in a way that the heavier sesquioxides are predicted to exist in the C phase, and for the lighter Ln_2O_3 the A phase is favored. This result is in very good agreement with the experimental data. However, both the PAW and the APW + lo methods underestimate the experimental $P_{C\to A}$ values. We relate these underestimations to the failure of these approaches in the description of the strongly correlated 4*f* electrons.

As mentioned above, the $P_{C\to A}$ dependence on Z_{Ln} can be understood by considering the possible more delocalized character of the Ln-4*f* orbitals in the A phase. In this respect, in the previous work of Petit et al. the valence state preference for Ln in Ln_2O_3 has been studied [29], and their calculations showed that all the sesquioxides prefer the trivalent configuration to the tetravalent one. In particular, they found that the Ln trivalence increases with Z_{Ln}, which is clearly related to the increasing localization of the *f* electrons.

When we applied the GGA + U approach, with $U = 0.8$ Ry to account for the strongly correlated Ln-4*f* electrons, we found that the predictions for V_0 are in excellent agreement with the experimental measurements. As we know, the GGA + U approach has also the capability to correctly indicate the insulator ground state for all the Ln_2O_3 series [31]. In our case, the Hubbard term also improves the predictions of V_0 with respect to those obtained with the previous approximations. Considering these features, this method emerges as a powerful tool to study the proposed systems. In this

respect, it is important to mention that in many systems the inclusion of the U parameter does not always improve the prediction of the structural properties. For example, the GGA + U calculations in LnO_2 systems presented in Ref. [27] show that the best agreement between the predicted equilibrium volume and the experimental value is obtained for $U = 0$ Ry, and the differences between these two values are larger as the U parameter is increased.

In this work we obtained excellent results for V_0, B, and B' by choosing $U = 0.8$ Ry for both the A and C phases of the studied sesquioxides. This choice seems to correctly balance the improvements of the GGA + U approach through all the Ln_2O_3 series. In particular, we found that the reason why for $U = 0.8$ Ry the V_0 predictions are in very good agreement with the experimental values is because of the degree of hybridization between Ln-4f and the O-2p states obtained with that correction. We showed that for the systems with a partially filled 4f band, a higher U leads to a weaker degree of hybridization, and the V_0 predictions asymptotically tend to values up to 3% higher than the experimental ones (remember the example of Fig. 9). If we consider that in the limit of very high U values the Ln-4f orbitals can be treated as core states, then we can compare our GGA + U results to those obtained using the CSM approach [26,56]. In that case, we can understand why when the Ln-4f shell are treated as a core-like shell, the GGA results obtained for V_0 are, in general, higher than the experimental ones (up to 6% higher [26]). We also tested the APW + lo method in the LDA + U approach, and we found that using high values for the Hubbard term the V_0 predictions asymptotically tends to values about 2% lower than the experimental ones. This result is in agreement with the LDA general underestimation of the experimental volumes previously obtained using the CSM approach [26].

On the other hand, we have shown that the $U = 0.8$ Ry choice gives very poor predictions for the $P_{C\rightarrow A}$ phase transition pressure. We showed that the prediction of $P_{C\rightarrow A}$ is extremely sensitive to the value of U: a slight change in U produces significant changes in $P_{C\rightarrow A}$. As we mentioned above, we arbitrarily chose the U value based in previous works, and only in order to tune the correct DOSs [31]. So, in order to improve the predictions for $P_{C\rightarrow A}$, we consider that a different methodology for selecting the Hubbard parameter is needed. Considering the observed response of E_0 upon a change in U for each phase, such methodology should depend on the structure. In this sense, a possible solution to this issue could be the choice of an alternative value for U from a structurally consistent method (i. e., the calculation of a phase structure and volume-dependent U, without recurring to the experimental data), such as that presented in Ref. [57]. We did not perform further calculations in this respect.

In summary, our results highlight the importance of considering the inclusion of a Hubbard parameter to obtain predictions of the structural and electronic properties of this kind of compounds in an overall agreement with the structural, mechanical, and conductivity experimental data. However, based on the response of each phase upon a change of the Hubbard term, we conclude that for the calculation of the phase transition pressure the methodology for selecting the U parameter must be revised.

Acknowledgments

This work was partially supported by Consejo Nacional de Investigaciones Científicas y Técnicas (CONICET) under Project No. PIP 0002. The research made use of the HP-Parallel-Computing Bose Cluster, and the computational facilities of the Physics of Impurities in Condensed Matter group, at Instituto de Física La Plata (IFLP) and Departamento de Física (UNLP).

References

[1] G. Adachi, N. Imanaka, Z.C. Kang (Eds.), Binary Rare Earth Oxides, Springer, New York, 2006.
[2] M. Fanciulli, G. Scarel (Eds.), Topics in Applied Physics 106: Rare Earth Oxide Thin Films, Springer, Berlin, 2007.
[3] A. Speghini, F. Piccinelli, M. Bettinelli, Opt. Mater. 33 (2011) 247.
[4] K. Kakushima, K. Tsutsui, S. Ohmi, P. Ahmet, V. Ramgopal Rao, H. Iwai, Top. Appl. Phys. 106 (2007) 345.
[5] M. Tang, J.A. Valdez, K.E. Sickafus, P. Lu, Appl. Phys. Lett. 90 (2007) 151907.
[6] L. Kittiratanawasin, R. Smith, B.P. Uberuaga, K.E. Sickafus, J. Phys. Condens. Matter 21 (2009) 115403.
[7] B.M.E. Russbueldt, W.F. Hoeldericha, J. Catal. 271 (2010) 290.
[8] V.B. Mortola, S. Damyanova, D. Zanchet, J.M.C. Bueno, Appl. Catal. B Environ. 107 (2011) 221.
[9] G. Adachi, N. Imanaka, Chem. Rev. 98 (1998) 1479.
[10] Matvei Zinkevich, Prog. Mat. Sci. 52 (2007) 597.
[11] W.R. Manning, O. Hunter, J. Am. Ceram. Soc. 52 (1969) 492.
[12] K.K. Phani, S.K. Niyogi, J. Am. Ceram. Soc. 70 (1987) C362.
[13] J. P. McClure, PhD thesis, University of Nevada, Las Vegas (2009).
[14] S. Jiang, J. Liu, C. Lin, L. Bai, Y. Zhang, X. Li, Y. Li, L. Tang, H. Wang, Solid State Comm. 169 (2013) 37.
[15] C. Hai-Yong, H. Chun-Yuan, G. Chun-Xiao, Z. Jia-Hua, G. Shi-Yong, L. Hong-Liang, N. Yan-Guang, L. Dong-Mei, K. Shi-Hai, Z. Guang-Tian, Chin. Phys. Lett. 24 (2007) 158.
[16] N. Dilawar, D. Varandani, S. Mehrotra, H.K. Poswal, S.M. Sharma, A.K. Bandyopadhyay, Nanotechnology 19 (2008) 115703.
[17] N.D. Sharma, J. Singh, S. Dogra, D. Varandani, H.K. Poswal, S.M. Sharma, A.K. Bandyopadhyay, J. Raman Spectr. 42 (2011) 438.
[18] Q. Guo, Y. Zhao, C. Jiang, W.L. Mao, Z. Wang, Solid State Comm. 145 (2008) 250.
[19] D. Lonappan, N.V. Chandra Shekar, P.C. Sahu, B.V. Kumarasamy, A.K. Bandyopadhyay, M. Rajagopalan, Philos. Mag. Lett. 88 (2008) 473.
[20] F.X. Zhang, M. Lang, J.W. Wang, U. Becker, R.C. Ewing, Phys. Rev. B 78 (2008) 064114.
[21] L. Bai, J. Liu, X. Li, S. Jiang, W. Xiao, Y. Li, L. Tang, Y. Zhang, D. Zhang, J. Appl. Phys. 106 (2009) 073507.
[22] D. Lonappan, N.C. Shekar, T.R. Ravindran, P.C. Sahu, Mater. Chem. Phys. 120 (2010) 65.
[23] N.D. Sharma, A.K. Bandyopadhyay, Raman spectroscopic studies of the rare earth sesquioxides and related compounds under high pressures, in: Z. Liu (Ed.), Rare Earths: New Research, Nova Science, 2013, ISBN 978-1-62808-014-8.
[24] S.D. Pandey, K. Samanta, J. Singh, N.D. Sharma, A.K. Bandyopadhyay, AIP Adv. 3 (2013) 122123.
[25] T. Atou, K. Kusaba, Y. Syono, T. Kikegawa, H. Iwasaki, in: Y. Syono, M.H. Manghnani (Eds.), High Pressure Research, Terrapub, Tokio, 1992, p. 469.
[26] M. Rahm, N.V. Skorodumova, Phys. Rev. B 80 (2009) 104105.
[27] M.B. Kanoun, A.H. Reshak, N. Kanoun-Bouayed, S. Goumri-Said, J. Magn. Magn. Mater 324 (2012) 1397.
[28] M. Shafiq, S. Arif, I. Ahmad, S. Jalali Asadabadi, M. Maqbool, H.A. Rahnamaye Aliabad, J. Alloys Compd. 618 (2015) 292.
[29] L. Petit, A. Svane, Z. Szotek, W.M. Temmerman, Phys. Rev. B 72 (2005) 205118.
[30] R. Gillen, S.J. Clark, J. Robertson, Phys. Rev. B 87 (2013) 125116.
[31] D. Richard, E.L. Muñoz, M. Rentería, L.A. Errico, A. Svane, N.E. Christensen, Phys. Rev. B 88 (2013) 165206.
[32] R.W.G. Wyckoff, in: Crystal Structures vol. 2, Wiley, New York, 1964. Chap. 5.
[33] P. Blaha, K. Schwarz, G. Madsen, D. Kvasnicka, J. Luitz, WIEN2k: an Augmented Plane Wave + Local Orbitals Program for Calculating Crystal Properties, Vienna University of Technology, Vienna, 2012.
[34] J.P. Perdew, Y. Wang, Phys. Rev. B 45 (1992) 13244.
[35] Z. Wu, R.E. Cohen, Phys. Rev. B 73 (2006) 235116.
[36] F. Birch, Phys. Rev. 71 (1947) 809.
[37] D. Richard, L.A. Errico, M. Rentería, Comp. Mat. Sci. 102 (2015) 119.
[38] V.I. Anisimov, J. Zaanen, O.K. Andersen, Phys. Rev. B 44 (1991) 943.
[39] V.I. Anisimov, I.V. Solovyev, M.A. Korotin, M.T. Czyzyk, G.A. Sawatzky, Phys. Rev. 48 (1993) 16929.
[40] R.C. Albers, N.E. Christensen, A. Svane, J. Phys. Condens. Matter 21 (2009) 343201.
[41] F. Hanic, M. Hartmanova, G.G. Knab, A.A. Urusovskaya, K.S. Bagdasarov, Acta Crystallogr. B 40 (1984) 76.
[42] K.K. Pandey, N. Garg, A.K. Mishra, S.M. Sharma, J. Phys. Conf. Ser. 377 (012006) (2012).
[43] S. Stecura, W.J. Campbell, Thermal Expansion and Phase Inversion of Rare-earth Oxides, Bureau of Mines Report No. 5847, United States Department of the Interior, Washington, 1961.
[44] S. Jiang, J. Liu, C. Lin, X. Li, Y. Li, J. Appl. Phys. 113 (2013) 113502.
[45] E.N. Maslen, V.A. Streltsov, N.A. Ishizawa, Acta Crystallogr. B 52 (1996) 414.
[46] Y. Makino, S. Miyake, J. Alloys Compd. 313 (2000) 235.
[47] S. Jiang, J. Liu, X. Li, L. Bai, W. Xiao, Y. Zhang, C. Lin, Y. Li, L. Tang, J. Appl. Phys. 110 (2011) 013526.
[48] P.C. Sahu, D. Lonappan, N.V.C. Shekar, J. Phys. Conf. Ser. 377 (2012) 012015.
[49] A. Saiki, H. Ishizawa, N. Mizutani, M. Kato, Yogyo Kyokaishi 93 (1985) 649.
[50] Q. Guo, Y. Zhao, C. Jiang, W.L. Mao, Z. Wang, J. Zhang, Y. Wang, Inorg. Chem. 46

(2007) 6164.
[51] S.L. Dole, O. Hunter, F.W. Calderwood, J. Am. Ceram. Soc. 60 (1977) 167.
[52] C. Meyer, J.P. Sanchez, J. Thomasson, J.P. Itie, Phys. Rev. B 51 (1995) 12187.
[53] S. Jiang, J. Liu, C. Lin, L. Bai, W. Xiao, Y. Zhang, D. Zhang, X. Li, Y. Li, L. Tang, J. Appl. Phys. 108 (2010) 083541.
[54] C.-M. Lin, K.-T. Wu, T.-L. Hung, H.-S. Sheu, M.-H. Tsai, J.-F. Lee, J.-J. Lee, Solid State Commun. 150 (2010) 1564.
[55] P. Haas, F. Tran, P. Blaha, Phys. Rev. B 79 (2009) 085104.
[56] N. Hirosaki, S. Ogata, C. Kocer, J. Alloys Compd. 351 (2003) 31.
[57] H. Hsu, K. Umemoto, M. Cococcioni, R. Wentzcovitch, Phys. Rev. B 79 (2009) 125124.